Supplementary information

Giant Thermal Conductivity in Diamane and the Influence of Horizontal Reflection Symmetry on Phonon Scattering

Liyan Zhu[1,2], Wu Li[3], and Feng Ding[2,4*]

I. Convergence tests

1. Energy cutoff

We first test the plane wave cutoff energy (E_{cut}) on the convergence of total energies and frequencies of highest optical phonon at the Γ point. The D-AB is selected as an example. When the E_{cut} is larger than 140 Ry, the variance of total energy is smaller than 1.0×10^{-4} Ry. As for the frequencies of optical phonons, the E_{cut} being larger than 150 Ry could make their variance within 0.1 cm^{-1}. Hence, the E_{cut} is set to be 150 Ry in the following calculations.

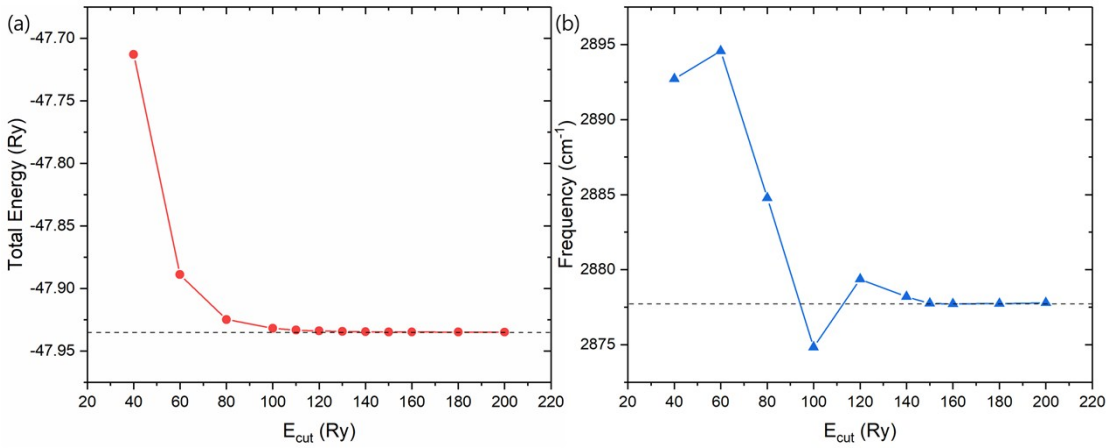

Figure S1. Effect of energy cutoff on (a) total energies and (b) frequencies of highest optical phonon at the Γ point.

2. K-point meshes for the electrons

We next the convergence of total energies and frequencies on the K-point meshes. When the K-point mesh being finer than 19×19×1 is adequate to make the variance of total energies and frequencies with 10^{-7} Ry and 0.05 cm^{-1}.

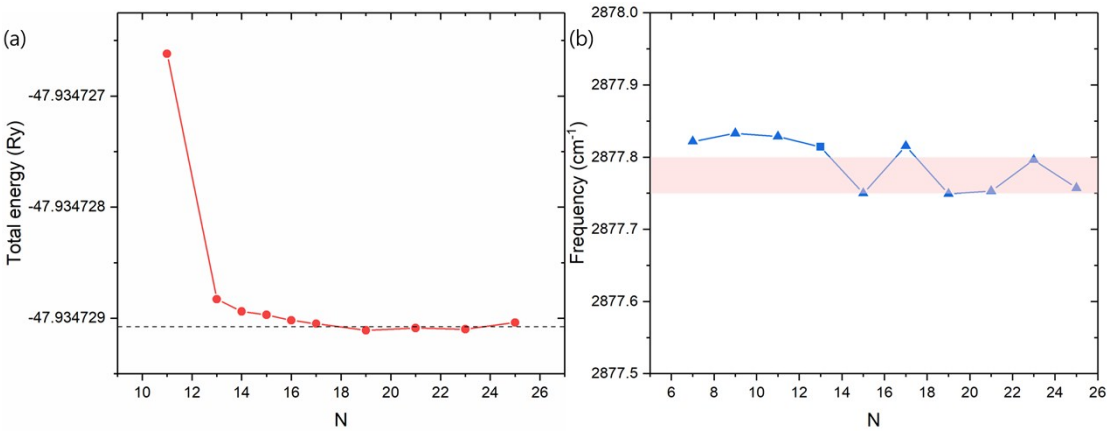

Figure S2. (a) Total energy and (b) frequency of highest optical phonon at the Γ point as a function of k-point meshes (**N**×**N**×1) employed in electronic self-consistent field calculations.

3. K-point meshes for phonons

To test the convergence with respect to the K-point meshes when solving Boltzmann transport equation, we directly calculate the thermal conductivities as a function of the K-point meshes as shown in Fig. S3. When the K-point meshes are 60×60×1, 70×70×1, and 80×80×1, the thermal conductivities are 1946.6, 1956.2, and 1958.8 W/m-K, respectively. So, the K-point mesh of 80×80×1 is a safe choice to get convergent thermal conductivity.

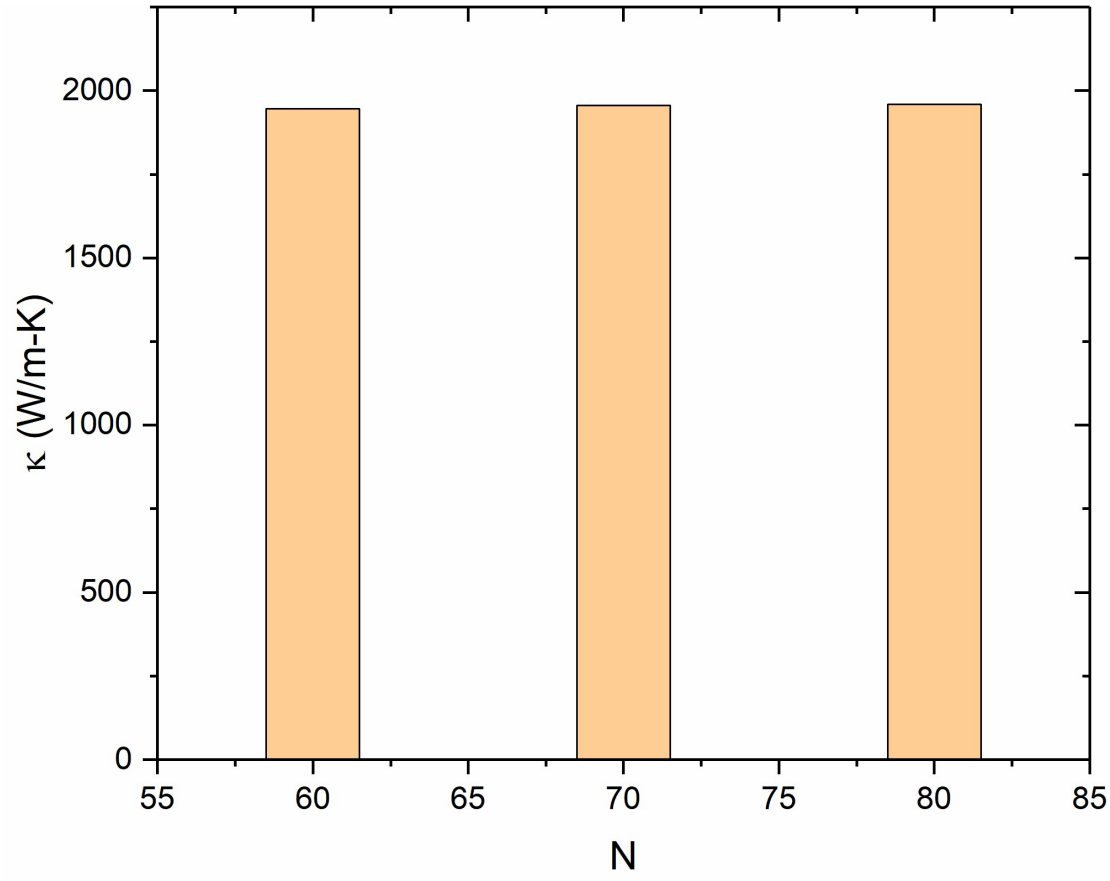

Figure S3. The thermal conductivities as a function of k-point meshes (**N**×**N**×**1**) for solving Boltzmann transport equations.

4. Convergence tests on second order force constants

To make sure the size of q-mesh is large enough during calculation of second force constants, we directly compare the phonon dispersion of D-AB with q-meshes changing from 7×7×1, 8×8×1, to 9×9×1. As shown in Fig. S4, the phonon dispersions are almost the same for all three cases. Hence, a q-mesh of 7×7×1 is large enough to guarantee the accuracy of second order force constants.

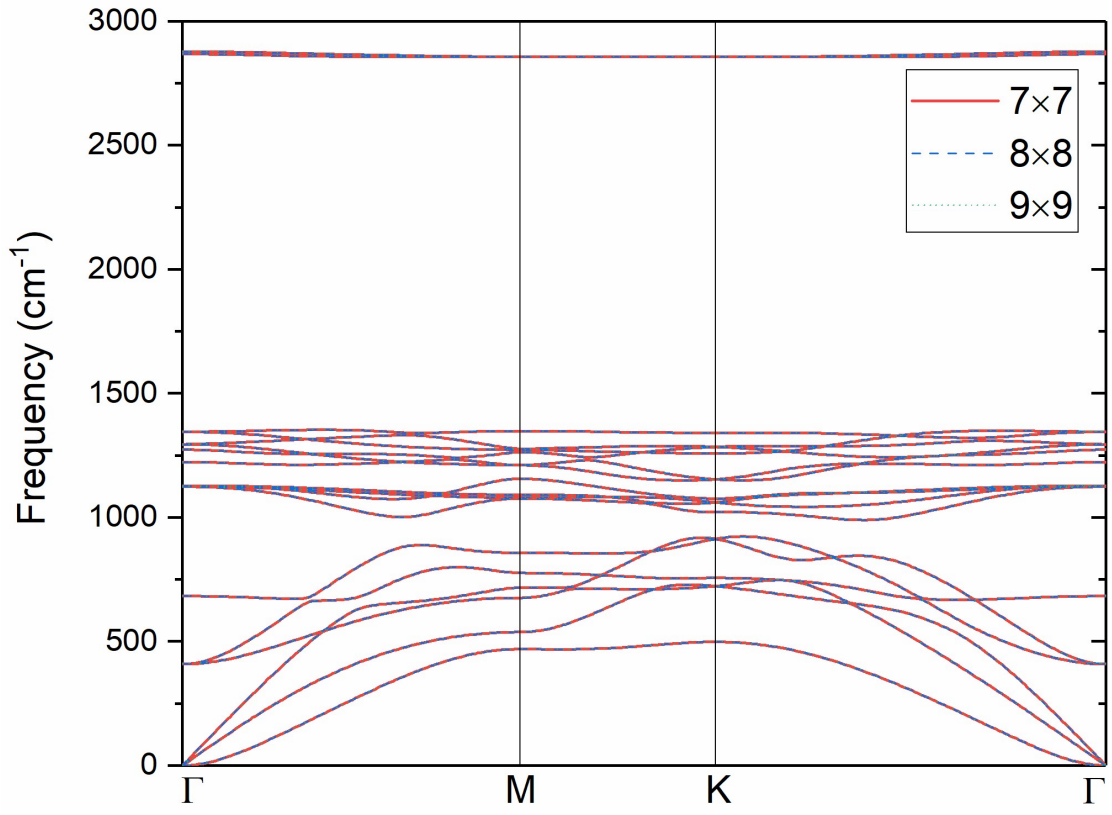

Figure S4. The effect of size of supercell on the phonon dispersion.

5. Convergence tests on third order force constants

To test the convergence on the size of q-mesh employed in calculating third order force constants, we compared the thermal conductivity of D-AB by using a 4×4×1 and a 8×8×1 q-mesh for the third order force constants, which are 1956.2 and 1969.8 W/m-K, of which the relative error is smaller than 0.7%. We also test the effect of q-meshes on the phonon line width for the 10th and 18th optical phonon at the Γ point as shown in Fig. S6. Apparently, the phonon line widths are almost the same for q-meshes of 4×4×1 and 8×8×1.

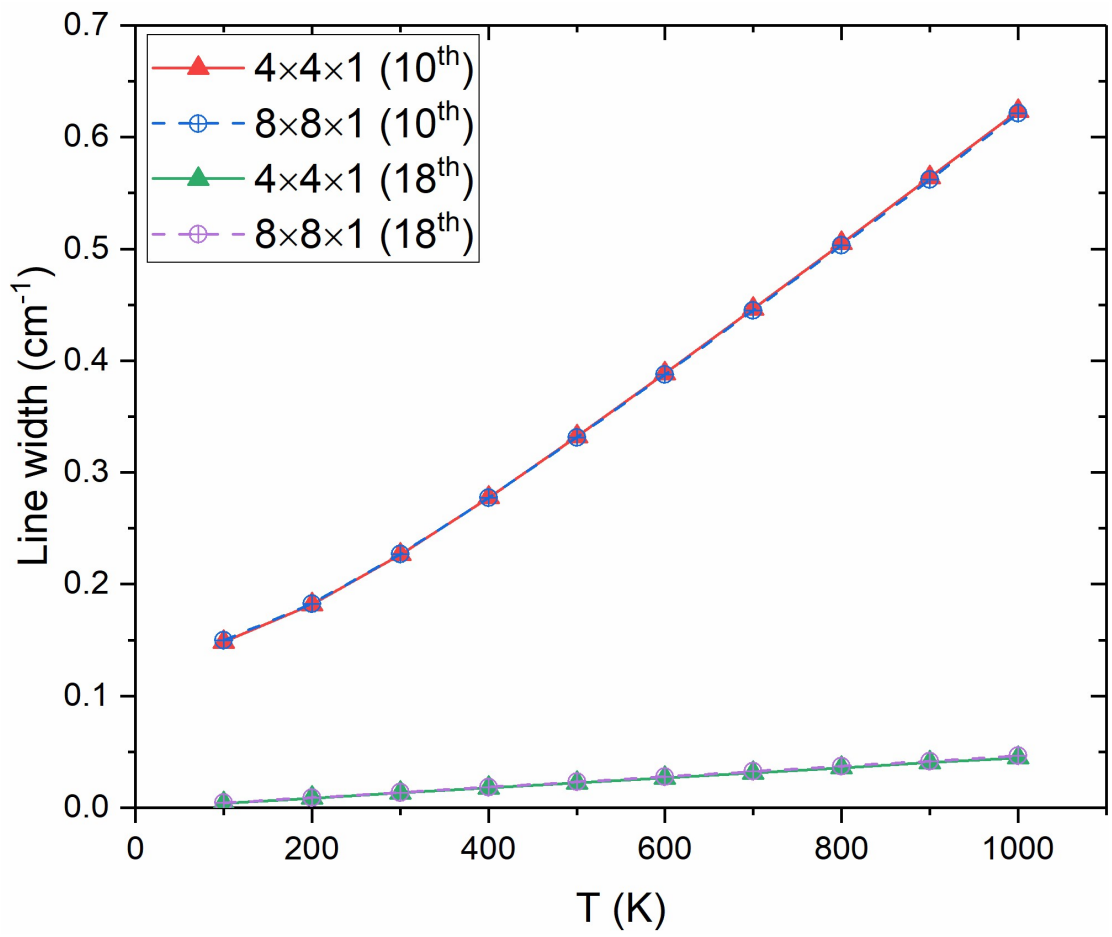

Fig. S5. Line width for the 10th and 18th branches of phonons at the Γ point versus the size of q-mesh employed to calculate third order force constants.

II. Distribution of scattering rates of a near-zone-center ZA phonon

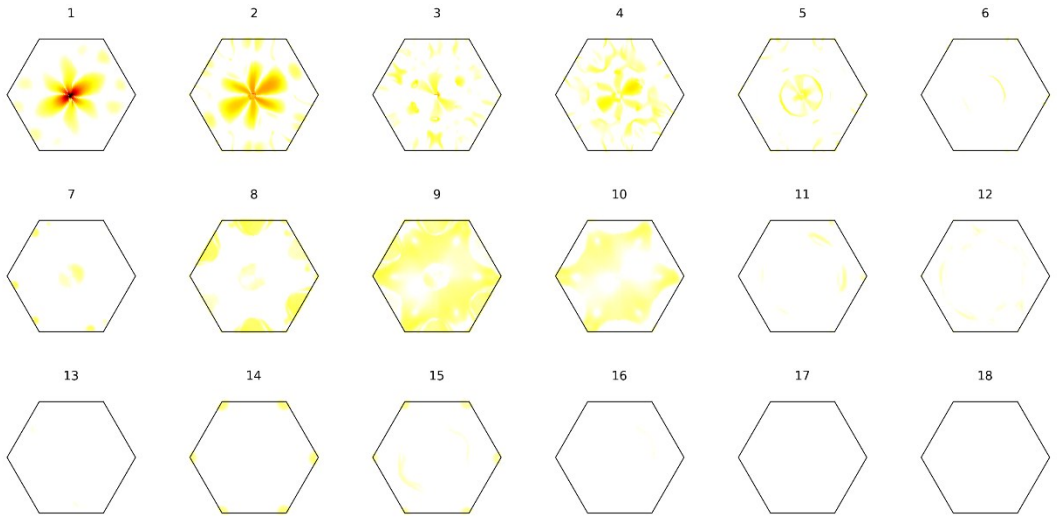

Figure S6. Distribution of scattering rates of a near-zone-center ZA phonon, ($\boldsymbol{q}_1$, ν_1) + ($\boldsymbol{q}_2$, ν_2) → ($\boldsymbol{q}_3$, ν_3), in Brillouin zone for D-AB, where $\boldsymbol{q}_1$ = (0.01, 0, 0) (in units of reciprocal lattice

vectors) and ν_1 = ZA. The ν_2 run over all 18 branches. In each panel, the scattering rates are summed over ν_3. The color bar is the same as that in Fig. 9.

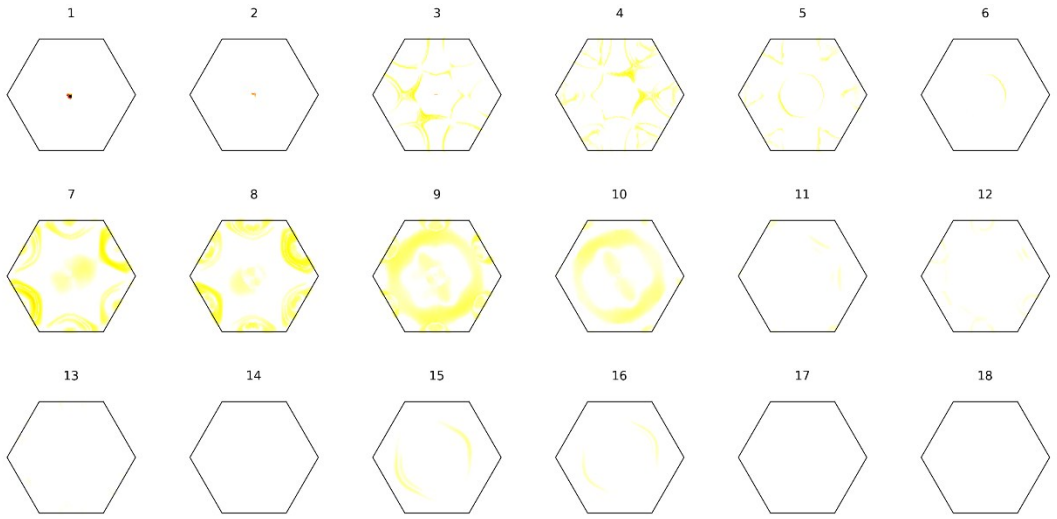

Figure S7. Distribution of scattering rates of a near-zone-center ZA phonon, ($\boldsymbol{q}_1$, ν_1) + ($\boldsymbol{q}_2$, ν_2) → ($\boldsymbol{q}_3$, ν_3), in Brillouin zone for D-AA, where $\boldsymbol{q}_1$ = (0.01, 0, 0) (in units of reciprocal lattice vectors) and ν_1 = ZA. The ν_2 run over all 18 branches. In each panel, the scattering rates are summed over ν_3. The color bar is the same as that in Fig. 9.

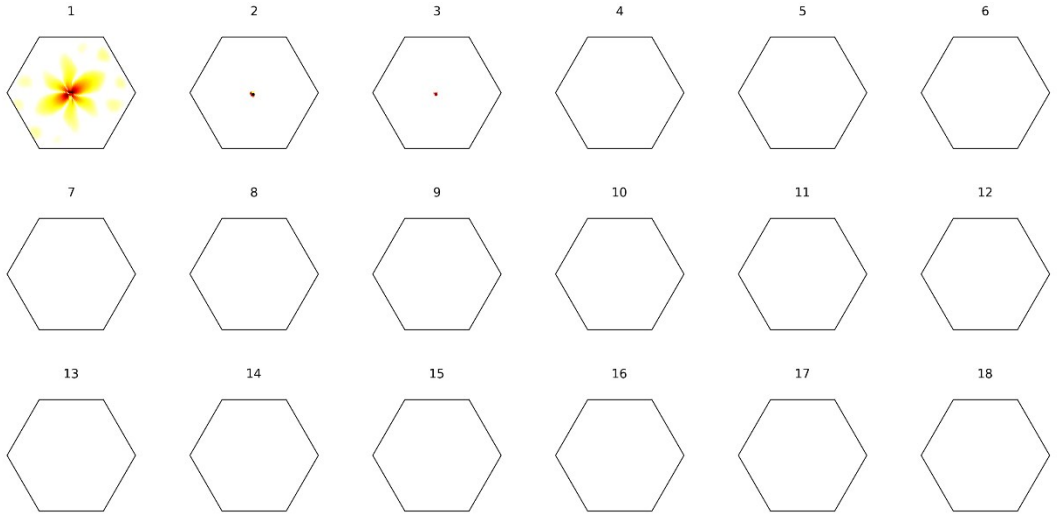

Figure S8. Distribution of scattering rates of a near-zone-center ZA phonon, ($\boldsymbol{q}_1$, ν_1) + ($\boldsymbol{q}_2$, ν_2) → ($\boldsymbol{q}_3$, ν_3), in Brillouin zone for D-AB, where $\boldsymbol{q}_1$ = (0.01, 0, 0) (in units of reciprocal lattice vectors), ν_1 = ZA, and ν_2 = ZA. The ν_3 run over all 18 branches. The color bar is the same as that in Fig. 9.

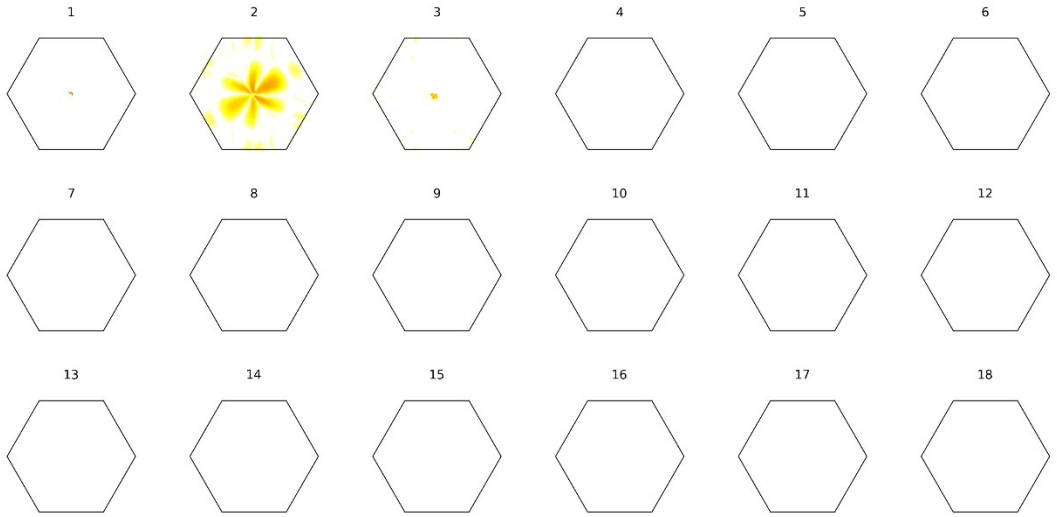

Figure S9. Distribution of scattering rates of a near-zone-center ZA phonon, ($\boldsymbol{q}_1$, ν_1) + ($\boldsymbol{q}_2$, ν_2) → ($\boldsymbol{q}_3$, ν_3), in Brillouin zone for D-AB, where $\boldsymbol{q}_1$ = (0.01, 0, 0) (in units of reciprocal lattice vectors), ν_1 = ZA, and ν_2 = TA. The ν_3 run over all 18 branches. The color bar is the same as that in Fig. 9.

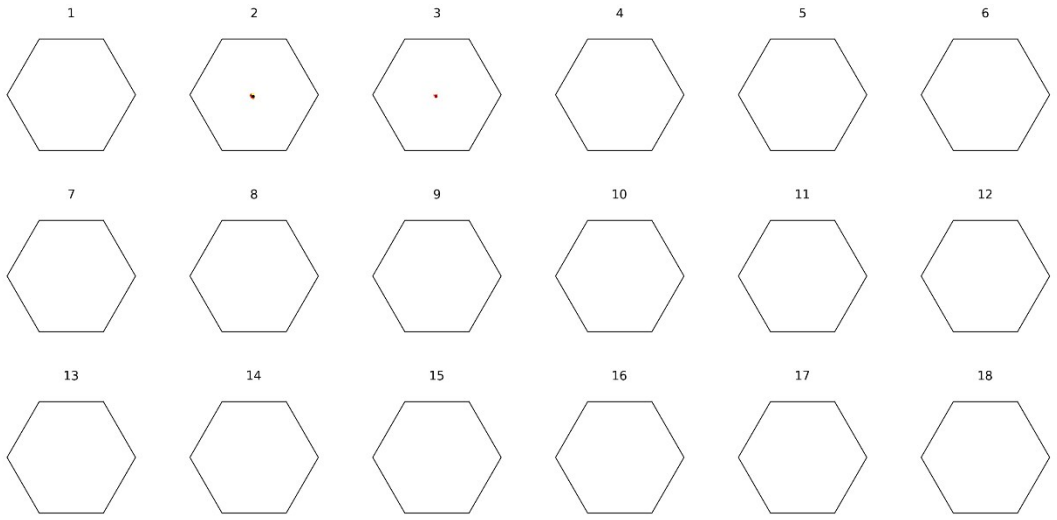

Figure S10. Distribution of scattering rates of a near-zone-center ZA phonon, ($\boldsymbol{q}_1$, ν_1) + ($\boldsymbol{q}_2$, ν_2) → ($\boldsymbol{q}_3$, ν_3), in Brillouin zone for D-AA, where $\boldsymbol{q}_1$ = (0.01, 0, 0) (in units of reciprocal lattice vectors), ν_1 = ZA, and ν_2 = ZA. The ν_3 run over all 18 branches.

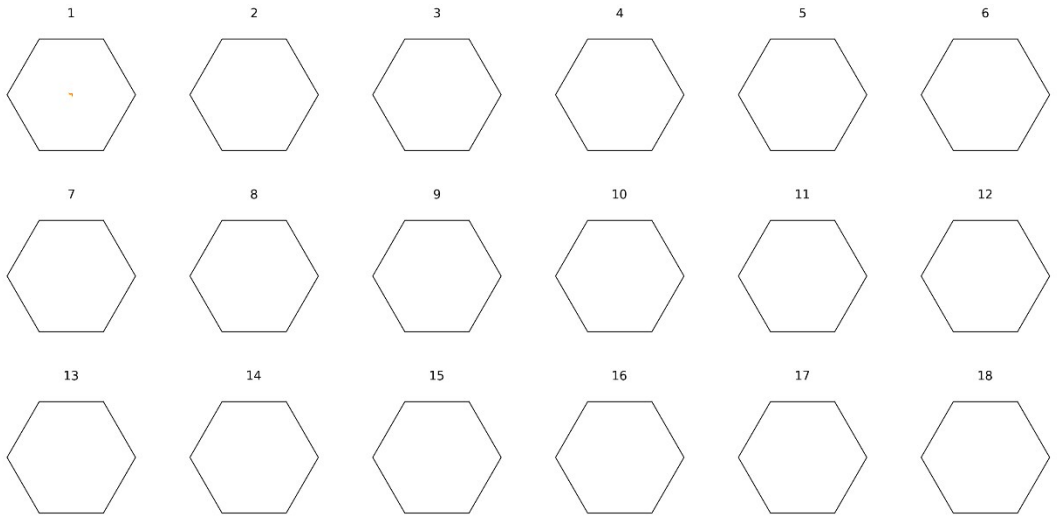

Figure S11. Distribution of scattering rates of a near-zone-center ZA phonon, ($\boldsymbol{q}_1$, ν_1) + ($\boldsymbol{q}_2$, ν_2) → ($\boldsymbol{q}_3$, ν_3), in Brillouin zone for D-AA, where $\boldsymbol{q}_1$ = (0.01, 0, 0) (in units of reciprocal lattice vectors), ν_1 = ZA, and ν_2 = TA. The ν_3 run over all 18 branches.